This article has been accepted for publication in a future issue of this journal, but has not been fully edited. Content may change prior to final publication. Citation information: DOI 10.1109/TPWRD.2015.2392386, IEEE Transactions on Power Delivery

Dynamic Thermal Modeling of a Voltage Divider Capacitive Coupling

C. Gonzalez, S. Weckx, *Member, IEEE*, T. De Rybel and J. Driesen, *Senior Member, IEEE*

***Abstract*-- This paper deals with the thermal model and compensation of the thermal drift in a capacitive voltage sensor installed on top of the semiconducting layer of a XLPE cable. The analysis of the thermal phenomena underlying the system shows a high dependency on the relative permittivity of the XLPE material. The first compensation method consists of installing an external capacitor with the same temperature coefficient as the cable capacitance. This method is limited because of the non-linear thermal behavior of the cable capacitance. The second method consists of measuring the conductor current and the outer XLPE temperature, and estimating the temperatures and properties of the cable by means of an off-line derived, built-in model. The simulations and tests show the obtained improvements of the different methods in the operational temperature range.**

***Index Terms*-- capacitive sensors, thermal analysis.**

I. Introduction

In recent years, Distribution Network Operators (DNO) have increased interest in installing voltage sensors in Medium Voltage (MV) networks. In the past, the voltage sensors in MV networks were mainly used both for protective relaying, installed at the feeder head, and for directional Fault Passage Indicators (FPI), installed at selected points along the feeder in order to minimize the outage time. However, the rising awareness for power quality issues, such as over- and under-voltage, unbalance and so on, and the need to measure the state of the grid for active network management is leading to the development of cost-effective voltage sensors. These voltage sensors should also be easy to install in an already existing grid, but also highly accurate, since power quality monitoring applications require this.

Several types of voltage sensors already exist on the market. Traditional voltage transformers are used in High Voltage (HV) grids, but they are too voluminous and expensive to be installed in very compact MV substations. Furthermore, the number of substations in the MV grid, in comparison with the substations in HV, is too large for this technology to be economically scalable. Another technology already existing in literature is the resistive voltage divider. This type of sensor requires a direct contact with the live conductor, and this is not always regarded as a feasible option. Also, their physical volume does not often allow retrofit.

A capacitive coupling can be obtained without direct contact with the live conductor, using a suitable insulation material between the conductor an electrode. Given the lack of contact, the capacitive coupling with the conductor can be achieved in many physical components of the electrical grid infrastructure. One solution consists of a capacitive coupling electrode that is attached to the elbow connector that connects the MV cable to the terminals of the MV/LV transformer. Another solution consists of a capacitive coupling from an electrode installed at the cable termination, becoming a coaxial capacitor. Similar solutions using such coaxial capacitive coupling on top of the cable insulation are described in [1]–[9]. The voltage sensors installed in the MV cable termination differ from the traditional CCVTs used for High-Voltage measurements. The CCVT voltage sensors contain a capacitive voltage divider, but also a conventional transformer in series, subject to a magnetization and saturation issues that have been largely studied, modeled and compensated, for instance in [10], [11].

In [1], the negative effects of contamination and moisture on the performance of capacitive voltage dividers at the grid frequency range is discussed. A novel technology is described in [1] to minimize such influence. It consists of introducing guarding electrodes at each side of the coupling electrode. The capacitive coupling in such sensor depends on the length of the measurement electrode, which in most practical cases will be of the order of tens of pico-Farads. Overall, the installation of such sensors must be very precise. Besides the installation issues, the accuracy of such sensors depends also on the cable insulation properties, which in this case is Cross Linked Poly-Ethylene (XLPE). At present, most of the underground cables that are newly installed are XLPE cables, replacing the old paper-lead or PVC cables. To increase the accuracy of such sensors, it is crucial to understand which factors are of major influence, so that they can be compensated or corrected. One of the major problems of this insulation material is the change of the relative permittivity with temperature [12]. Therefore, the sensors based on this type of capacitive coupling may include a thermal compensation mechanism.

In section II of this paper, the geometry of the voltage sensor embodiment is described, as well as the basic calculations for the coaxial capacitive coupling. In section III,

This work was supported by the KIC - Active SubStations project, from the European Institute of Technology (EIT).

C. Gonzalez, S. Weckx and J. Driesen are with the Department of Electrical Engineering ELECTA/ESAT, Katholieke Universiteit Leuven, Kasteelpark Arenberg 10, bus-2445, Heverlee, B-3001, Belgium. Sam Weckx and has a PhD fellowship of the Research Foundation - Flanders – VITO (FWO-VITO) (e-mail: carlos.gonzalezdemiguel@esat.kuleuven.be).

T. De Rybel is with KIC-Innoenergy, Eindhoven, Netherlands.

This article has been accepted for publication in a future issue of this journal, but has not been fully edited. Content may change prior to final publication. Citation information: DOI 10.1109/TPWRD.2015.2392386, IEEE Transactions on Power Delivery

the thermal processes underlying cable heating will be explained, including the heat transfer modes, the thermal linear expansion and the change of relative permittivity of the XLPE.

Two methods are proposed to compensate the capacitance thermal drift. The first method, in section V, aims to construct a voltage divider where the two impedances have the same thermal drift. This requires a thermal characterization of the capacitive coupling in the operational temperature range, so that the compensating passive component has the same thermal drift. This method is commonly applied in integrated circuits design and microelectronics. The thermal drift of the capacitive coupling will be determined both experimentally and analytically.

The second method, in section VI, aims to compensate the thermal drift digitally in a micro-processor in a further stage of the voltage sensor. It consists of estimating the temperatures inside the XLPE layer to determine the actual value of its relative permittivity, while also evaluating the other thermal phenomena. Most of the literature related to temperature estimation inside the cable is for ampacity optimization purposes [14]–[16] or for ageing and degradation purposes [17]. Most of them use multi-physics software to solve the coupled problem and determine the internal distribution of temperature, using finite elements or finite differences, amongst other techniques [18]. Estimating the temperature by such detailed models is unfeasible for product implementation purposes. Instead, in this paper, the Dynamic Compact Thermal Model (DCTM or CTM) is determined analytically. For the temperature estimation, the Cauer model is applied, also known as thermal-electrical analogy, leading to a linear RC circuit that can be solved without high computational requirements. The cable capacitance is tested under realistic conditions, which allows the comparison of the performance of the different compensation methods.

II. Capacitive Coupling Of A Voltage Divider

The capacitive coupling of study within this paper is constructed inside a MV cable termination, using a cable of type: Eupen EAXeCWE 8.7/15kV 1x240, where the outer PE sheath, the copper earthing wires, and the anti-moisture layers have only been removed in the termination.

The outer semi-conductive layer is used for field control in the XLPE insulation. For mechanical installation of the sensor, it is still necessary to secure the electrodes and, therefore, a wrapping compressive plastic layer is installed on top of the electrode. Moreover, a cold shrink termination is installed to cover the whole, as shown in Fig. 1 and 2.

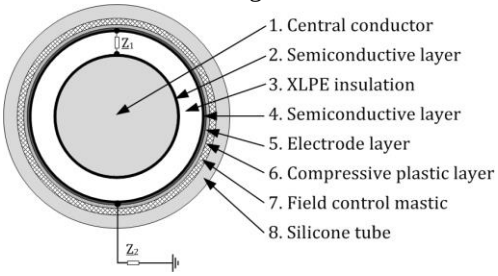

Fig. 1. Radial Cross section of the termination assembly

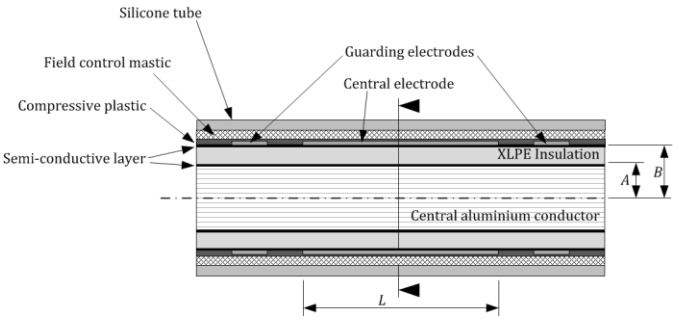

Fig. 2. Axial cross section of the termination assembly

This termination is installed for field control purposes, but also for protection and also to avoid the penetration of moisture and pollution [19], [20]. The cold shrink termination consists of two layers: an inner field or stress control mastic and a silicone tube. The impedance of the coupling will be named $\underline{Z}_1$, where the capacitance of $\underline{Z}_1$ will be named C_1. In order to create the voltage divider, a second impedance $\underline{Z}_2$, in this case a capacitance C_2, needs to be included in the circuit, one side connected to the electrode and to the ground in the other side. The impedance $\underline{Z}_2$ is to be chosen by the manufacturers. The general formulation of the voltage divider, resistive or capacitive, is expressed in the terms of

$$\underline{V}_{out} = \frac{\underline{Z}_2}{\underline{Z}_1 + \underline{Z}_2} \cdot \underline{V}_{in} \tag{1}$$

Where $\underline{V}_{in}$ is the voltage signal to be estimated and $\underline{V}_{out}$ is the output signal. Consider the full scheme of the capacitive voltage divider in Fig. 3, where the cable impedance ($\underline{Z}_1$) consists of a conductance (G_{cable}) and a capacitance (C_{cable}), and the external passive capacitor ($\underline{Z}_2$) is modeled as a capacitive part (C_2), its Equivalent Series Resistance ($R_{2,ESR}$) and the Equivalent Series Inductance ($L_{2,ESL}$).

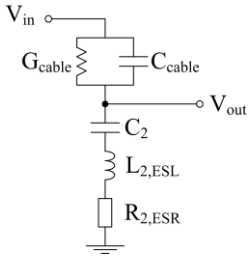

Fig. 3. Full impedance model of the capacitive voltage divider

Regarding the circuit lumped elements in Fig. 3, several simplifications can be made when working at grid frequency, as it is the case in this paper. The cable impedance is mostly capacitive and leads to a capacitive charging current in AC regimes, calculated as

$$I_C = 2\pi f C_{cable} E \tag{2}$$

Where I_C is the capacitive charging current, f is the grid frequency, C_{cable} is the cable capacitance and E is the grid voltage. Since all the insulation materials are imperfect, a resistive current is also present, modeled as conductance, and it is considered as insulation losses. Instead of calculating the losses in terms of conductance, the dissipation factor, power factor or $tan\delta$, are the more usual terminology.

This article has been accepted for publication in a future issue of this journal, but has not been fully edited. Content may change prior to final publication. Citation information: DOI 10.1109/TPWRD.2015.2392386, IEEE Transactions on Power Delivery

$$I_R = 2\pi f C_{cable} E \tan\delta \tag{3}$$

Where I_R is the resistive part of the capacitive charging current. For XLPE cables, tan values are rather low, between 0.005 and 0.02 [13]. The current paper deals with XLPE cables under low frequency conditions and, therefore, this resistive part will be omitted. Regarding the external capacitor ($\underline{Z}_2$), the ESR in ceramic capacitors is estimated below 0.015 Ω, whereas the actual value of the capacitance is foreseen as 150nF. This means that at a grid frequency of 50Hz, the ESR impedance is about $1 \cdot 10^{-7}$ times the capacitive reactance and therefore, it can be neglected from the scheme. The ESL in ceramic capacitances is estimated below 3nH, leading to an inductive reactance at 50Hz of about $4 \cdot 10^{-11}$ Ω and, hence, it will also be neglected from the full impedance circuit. As a result of the previous assumptions, it is assumed that the impedances $\underline{Z}_1$ and $\underline{Z}_2$ are purely capacitive, so that (1) becomes

$$\underline{V}_{out} \approx \frac{C_1}{C_1 + C_2} \cdot \underline{V}_{in} \tag{4}$$

Moreover, since C_2 is significantly larger than C_1, (4) can be further approximated to

$$\underline{V}_{out} \approx \frac{C_1}{C_2} \cdot \underline{V}_{in} \tag{5}$$

Given the electrode geometry, the assembly acts as a coaxial, cylindrical capacitor C_1, whose capacitance is calculated as

$$C_1 = \frac{2\pi\varepsilon_0\varepsilon_r}{\ln(B/A)} \cdot L \tag{6}$$

The parameters *A*, *B* and *L*, refer to the electrode geometry and are indicated in Fig. 2. ε_0 is the vacuum permittivity, equal to $8{,}854 \cdot 10^{-12}$ F/m and ε_r is the relative permittivity of the insulation layer. By determining the value of the ratio of capacitances in (4), it is possible to estimate $\underline{V}_{in}$ from $\underline{V}_{out}$. Most of the parameters required for the voltage conversion between the input and output signals are temperature dependent, and, therefore, it is necessary to introduce the thermal phenomena underlying the voltage sensor.

III. Thermal Processes

Multiple thermal processes are involved in the voltage sensor embodiment, such as the linear thermal expansion, the heat generation inside the central conductor, and the heat capacity and transfer within the different layers of the geometry. The heat conduction has been studied by means of the cylindrical solid body heat transfer in one dimension [21]. The application of this model implies the use of the cross section geometry parameters illustrated in Fig. 1 and 2. Another important thermal process is the change of relative permittivity of the XLPE.

A. Heat Generation

The heat generation is due to the dissipated power because of the Joule effect, where the losses are expressed as

$$\Delta Q / \Delta t = P_{losses} = R \cdot I_{RMS}^2 \tag{7}$$

Where $\Delta Q/\Delta t$ is the generated rate of heat flow, equal to the power losses, P_{losses}. R is the resistance of cable section and I_{RMS} is the Root Mean Square current through the cable. However, the resistance of the conductor is also dependent on the temperature, according to

$$R_{\theta 2} = R_{\theta 1}\left[1 + \alpha_{Al}\left(\theta_2 - \theta_1\right)\right] \tag{8}$$

Where $R_{\theta 1}$ and $R_{\theta 2}$ are the resistance at the temperatures θ_1 and θ_2 and α_{Al} is the coefficient of variation of the resistance with temperature, which depends on the material (Aluminum in this case). The combination of (7) and (8) leads to

$$\Delta Q / \Delta t = R_{20}\left(1 + \alpha_{Al,20}\left(\theta_2 - 20\right)\right) \cdot I_{RMS}^2 \tag{9}$$

Within this paper, the reference temperature is 20°C, and the material Aluminum therefore, R_{20} is the resistance of the conductor at this temperature.

B. Heat Conduction

The heat conduction from layer to layer is given by the equations for heat transfer in a cylindrical body, governed by

$$\theta_1 = \theta_0 + \frac{\Delta Q / \Delta t \cdot \ln\left(r_0 / r_1\right)}{2\pi k L} \tag{10}$$

Where θ_1 is the outer temperature and θ_0 is the inner temperature, according to the chosen convention. $\Delta Q/\Delta t$ is the rate of heat flow in [W], r_0 and r_1 are the corresponding inner and outer radii. k is the thermal conductivity [W/m·K] and L is the axial length [m]. The thermal conduction mode applies from the central aluminum conductor till the second-to-last layer, inside the cable external insulation. The temperature distribution inside the central conductor requires a different calculation with the Byot model, not considered in this paper.

C. Heat Capacity

The heat capacity refers to the ability of storing heat in the material. It is important for the study of transients and thermal dynamics. It is defined as

$$C_h = \frac{\Delta Q}{\Delta \theta} \tag{11}$$

The heat capacity (C_h) is a volumetric and mass property. For this reason, when modeling the stored heat in the different layers, it is required to take into account both the geometrical change and the density. For the study of the sensor embodiment, only the volume contained inside the electrode geometry will be considered.

D. Other Heat Transfer Modes

Within this paper, it will be assumed that any thermal compensation method works at the outer XLPE layer temperature. This implies that the phenomena that take place in the outer layers of the cable, such as radiation or convection with the surrounding air, are considered out of the scope of this description.

E. Linear Thermal Expansion

The elastic deformation of the materials inside the embodiment is given by the linear thermal expansion equation

This article has been accepted for publication in a future issue of this journal, but has not been fully edited. Content may change prior to final publication. Citation information: DOI 10.1109/TPWRD.2015.2392386, IEEE Transactions on Power Delivery

$$L_{\theta 2} = L_{\theta 1}\left[1+\sigma_L\left(\theta_2-\theta_1\right)\right] = L_{\theta 1}\cdot\left(1+\sigma_L\Delta\theta\right) \quad (12)$$

Where $L_{\theta 2}$ and $L_{\theta 1}$ are the lengths of the body at temperatures θ_2 and θ_1, $\Delta\theta$ is the given temperature increment, respectively, and σ_L is the linear thermal expansion coefficient [m/m·K] of the electrode material. The axial deformation leads to an increase of the capacitor length *L*. The application of the linear thermal expansion to the XLPE layer in axial dimensional, the ratio of radius between the outer side of the aluminum central conductor and the inner capacitor plate is defined by

$$\left(\frac{B'}{A'}\right) = \left(\frac{A\cdot(1+\sigma_A\Delta\theta_A)+(B-A)\cdot(1+\sigma_{XLPE}\,\overline{\Delta\theta}_{XLPE})}{A\cdot(1+\sigma_A\Delta\theta_A)}\right) \quad (13)$$

B' and *A'* are the dimensions of the XLPE at the new temperature. Combining equations (6), (12) and (13), and applying also the axial deformation in the central capacitor, results in

$$C_1 = \frac{2\pi\varepsilon_0\varepsilon_r\cdot L\cdot\left(1+\sigma_L\Delta\theta\right)}{\ln\left(1+\frac{B-A}{A}\cdot\frac{1+\sigma_{XLPE}\,\overline{\Delta\theta}_{XLPE}}{1+\sigma_A\Delta\theta_A}\right)} \quad (14)$$

F. Relative Permittivity Thermal Change

The relation between temperature and relative permittivity is shown in Fig. 4 [12].

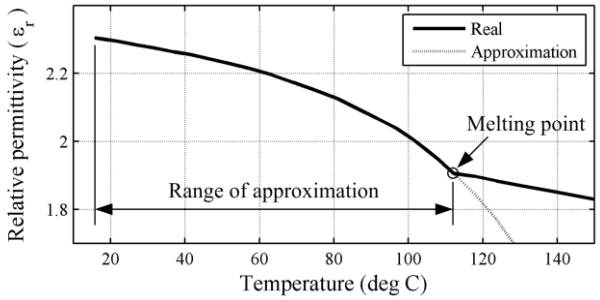

Fig. 4. XLPE relative permittivity dependent on temperature

The temperature range of normal operation requested from a voltage sensor does not exceed 90 ˚C. Towards the compensation of the measurements in a digital processor in a further stage of the sensor, below the melting point, around 110 ˚C, the curve from Fig. 4 has been digitized. Towards the implementation in a signal processor, it is possible to approximate the curve, as in (15), or to make use of a look-up table and interpolate further.

$$\varepsilon_{r,XLPE}(\theta) \approx \alpha\cdot e^{\beta\cdot\theta} + \gamma\cdot e^{\delta\cdot\theta} \quad (15)$$

Given the heat conduction mechanism in a cylindrical body, (16) relates the radius of the cylinder with its temperature

$$\frac{\theta_x-\theta_i}{\theta_0-\theta_i} = \frac{\log(r_x/r_i)}{\log(r_0/r_i)} \quad (16)$$

From equation (16) it can be observed that temperature at the inner side of the XLPE layer is different than the temperature at the outer side of the same layer. This temperature difference leads to a difference in the relative permittivity of the material, between both sides of the layer. Towards the calculation of the cable capacitance, an equivalent, unique value of the relative permittivity is taken. This value is found considering (i) the approximation formula to the relative permittivity in equation (15), (ii) the fact that there is less XLPE material in the inner side of the layer and (iii) the temperature distribution in a cylindrical body, defined by equation (16).

The XLPE cross section layer has been discretized in 1000 small radius increments (Δx), as shown in Fig. 5 (a). The values of the XLPE relative permittivity have been estimated for all steps along the XLPE layer thickness, according to (15). The spatial discretization and the relative permittivity at each radial step are plotted in Fig. 5.

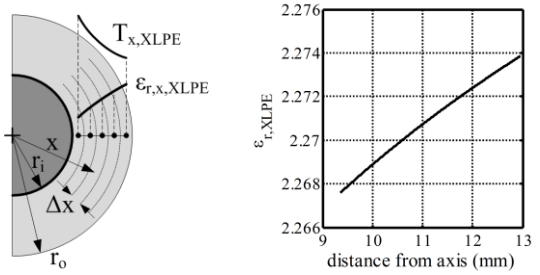

Fig. 5. XLPE relative permittivity and temperature profile along the radial direction of the XLPE insulation layer. (left) Discrete integration parameters. (right) Simulated profile, when the difference of temperatures θ_1-θ_0 is about 3 degrees.

Where r_i and r_o are the inner and the outer XLPE radius, Δx is the radial discrete increment. The integration is done by

$$\bar{\varepsilon} = \frac{\sum_x \varepsilon_x\cdot\pi\left(\left(x+\frac{\Delta x}{2}\right)^2-\left(x-\frac{\Delta x}{2}\right)^2\right)}{\pi\left(r_0^2-r_i^2\right)} \quad (17)$$

$\bar{\varepsilon}$ being the average relative permittivity along the whole thickness of the XLPE layer. After reduction, (17) becomes

$$\bar{\varepsilon} = \frac{\sum_x \varepsilon_x\cdot 2\cdot x\cdot\Delta x}{r_0^2-r_i^2} \quad (18)$$

G. Combining the thermal processes

From (14) it is observed that the capacitance depends linearly on the relative permittivity and the electrode length and depends inversely on the logarithm of *B/A*. The variation of these magnitudes has been evaluated between 20 ˚C and 90 ˚C in steady-state conditions, without heat flux (Table I). The variation of the parameters leads to a variation in the capacitance (ΔC_1).

TABLE I
Relative Change of Variables (Δ) between 20 and 90 ˚C and influence on the capacitance (ΔC_1)

Parameter	**20 °C**	**90 °C**	**Δ (%)**	**ΔC_1 (%)**
L [mm]	45	45.052	0.116	+0.116
B/A	1.385	1.399	1.013	-
1/ln(B/A)	3.0703	2.9783	-0.0920	-0.0920
$\varepsilon_{r,XLPE}$	2.298	2.078	-9.556	-9.556

This article has been accepted for publication in a future issue of this journal, but has not been fully edited. Content may change prior to final publication. Citation information: DOI 10.1109/TPWRD.2015.2392386, IEEE Transactions on Power Delivery

On the one hand, from Table I it can be seen that when temperature increases, the change of the electrode length leads to a larger capacitance. On the other hand, when the temperature increases, the changes in the relative permittivity and the cross section radius lead to a smaller capacitance. The influence of the geometry (electrode length and cross section radius) is very small in comparison with the relative permittivity. Hence, the changes in the capacitance are mostly driven by the changes in the relative permittivity. Being C_1 proportional to $\varepsilon_{r,XLPE}$, the capacitance is expected to vary similarly as in Fig. 4. However, the model herein described considers all the thermal phenomena, which are combined sequentially as in the flowchart in Fig. 6.

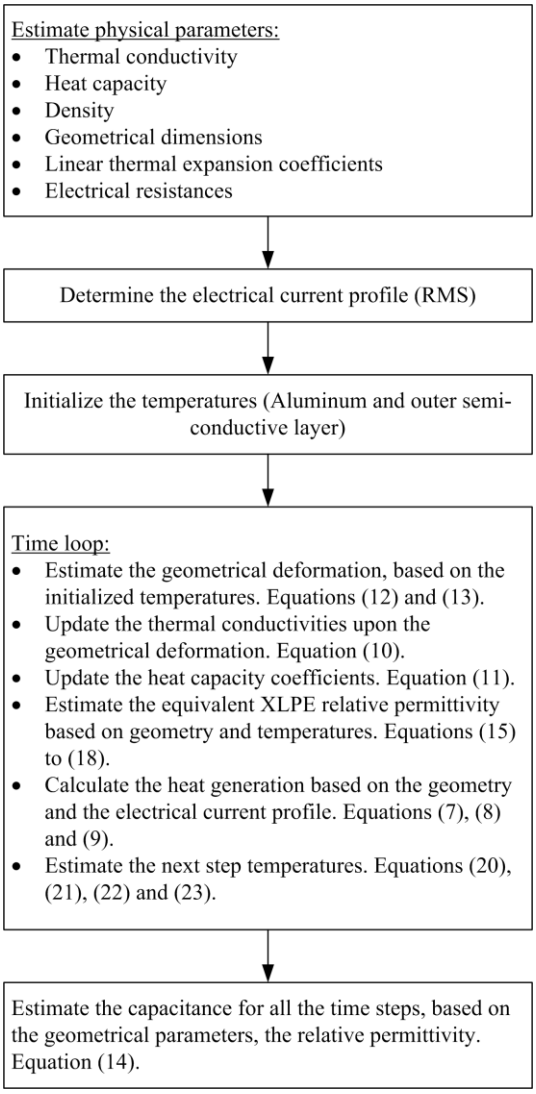

Fig. 6. Calculation flowchart to combine all the thermal phenomena presented in the previous subsections.

IV. Experimental Measurements

The change of capacitance while current flows through the cable has been measured, as well as the temperatures on both sides of the XLPE insulation. Figure 7 shows the 1 m cable where 2 miniature thermocouples have been drilled at different depths (outer and inner XLPE layer depth), spaced 40 cm from each other. The cable has been enclosed in a box, to simulate a closer environment, similar to an MV sub-station cable compartment.

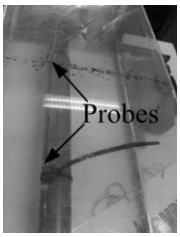

Fig. 7. Thermal probes attached to the cable. Inner and outer side of the XLPE insulating layer.

The impedance analyzer used for the capacitance measurements was an HP 4262A LCR Meter. The capacitance was measured with a frequency of 10 kHz. The impedance analyzer measures the capacitance of the whole cable (1 m) at about 388 pF. 4-terminals Kelvin connections were used throughout. The impedance analyzer is set-up to measure the capacitance assuming a RC-parallel circuit, as it is often assumed when modelling the cable insulation (see Fig. 3). For the cable capacitance range, the manufacturer specifies a basic accuracy of 0.2% and 0.3%.

Three steps of 50 Hz current were applied to the cable: 200 A, 300 A and 0 A were set up to heat up the cable and cool it down. In Fig. 8, the measured temperatures are plotted in time, while applying different step currents through the conductor. Such measurements were taken every 15 seconds.

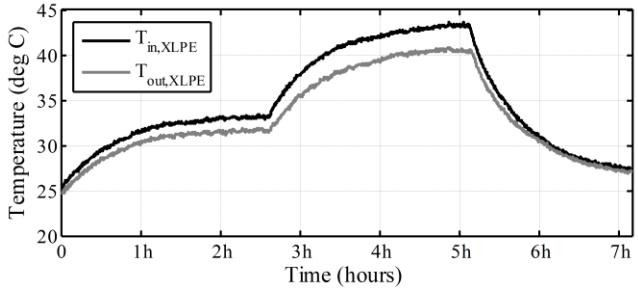

Fig. 8. Temperatures measured at the inner and outer sides of the XLPE insulation layer of the cable

The temperature measurements at the outer semi-conductive and XLPE layer are important for the calculation of the total relative permittivity of the XLPE. First, in Fig. 5, it can be seen that the XLPE insulation layer is not at a homogeneous temperature. Moreover, the difference of temperatures between the two sides depends on the electrical current flowing through the conductor, as the generated heat is quadratically related to such current. For this reason, a more accurate estimation of the XLPE relative permittivity should include the temperature on both sides.

The measured capacitance during the previous test is plotted in Fig. 9. The variations in the capacitance are introduced by the impedance analyzer and its difficulties to measure such tiny values of the capacitance, which are in the order of a few tens of pico-farads. A zero-phase filter with a window of 15 samples has been applied to partially remove such variations. The filtered signal is used as reference case.

This article has been accepted for publication in a future issue of this journal, but has not been fully edited. Content may change prior to final publication. Citation information: DOI 10.1109/TPWRD.2015.2392386, IEEE Transactions on Power Delivery

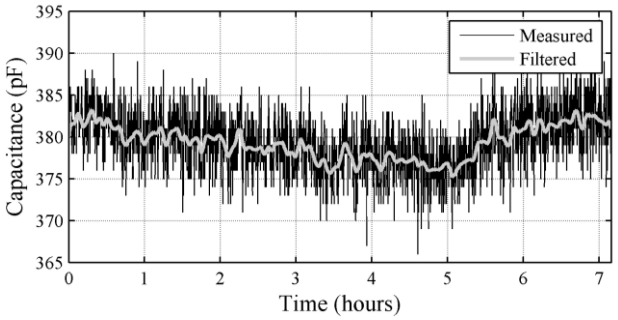

Fig. 9. Measured capacitance when applying the current steps

It can be seen that the capacitance changes slightly more than 2 % over the covered range of measurements from 25 ˚C to 43 ˚C. This change of capacitance directly affects the voltage measurement if it is not compensated. Following the temperature profiles in Fig. 8, in general terms, the higher the temperature, the lower the capacitance, as predicted in subsection III-G. When the current flow is stopped, the heat is redistributed between all the layers, leading to a quick descent of the temperatures and the rise of the capacitance back to the initial value.

V. Compensation Method 1

In [1], it is suggested to select C_2 with a specific thermal drift characteristic, so that it can compensate all the phenomena above-explained. This passive technique would not require any further digital signal compensation. Such capacitor C_2 should be allocated close to the electrode, so that the capacitor is still sensitive to the outer XLPE temperature. Towards the selection of the compensating capacitor C_2, the temperature drift of such passive components is defined by means of the Temperature Coefficient of Capacitor (TCC) in terms of *ppm* (parts-per-million) per degree Celsius, over the rated value of the capacitance at 25 ˚C. The TCC is calculated as in (19), and refers to linear thermal drift capacitors.

$$TCC_{C1} = \frac{\Delta C_1}{\Delta \theta} \cdot \frac{10^6}{C_{1,25^\circ C}} \tag{19}$$

In Fig. 10, the coupling capacitor is plotted as a function of the outer XLPE temperature, from the measurements introduced in Fig. 8.

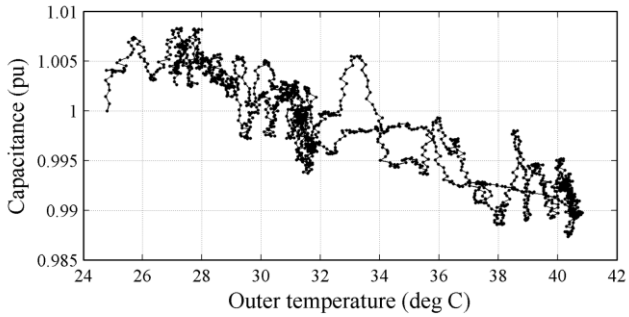

Fig. 10. Capacitive coupling as function of the electrode temperature

The realized tests only cover the range of electrode temperature from 24 to 41 ˚C. This compensation method will be illustrated in this narrow range.

Recall that the ultimate purpose is to flatten the ratio of capacitances (4) over the temperature range as much as possible, by finding the slope of the capacitance change. Least Squares regression is sensitive to the sample concentration and is not a suitable technique for this analysis.

A. Results

The appropriate TCC coefficient has been found by sweeping the TCC coefficient till the minimum range of the capacitances ratio was obtained. Finding the TCC with this technique is sensitive to outliers. However, the prior knowledge about the shape of the curve and its pattern makes these easy to detect. Furthermore, the removal of the outliers may not affect the accuracy since the method is not strictly dependent on the amount of samples. Such analysis leads to determine a TCC approximated to -805 *ppm* (or N805). Considering the error of the measurement instrument This specific temperature coefficient is not commercially available and, therefore, in order to obtain such coefficient, it is necessary to combine two or more capacitors in parallel with different TCCs, for instance, one of N750 and another without thermal drift, for instance N1000, weighted, so that the combination behaves thermally as desired. Recall that a compensating capacitor C_2 of 150 *nF* is assumed.

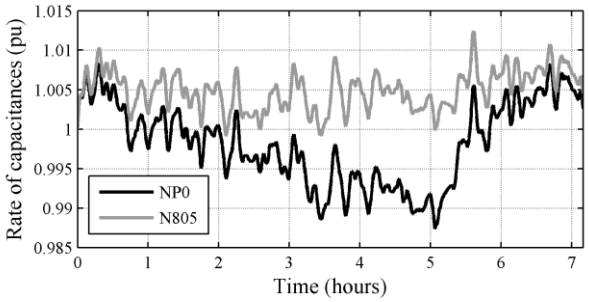

Fig. 11. Ratio of capacitances, in pu, from (4) when *C2* is NP0 and N805.

The improvement using this technique is evaluated with a capacitor C_2, without thermal drift, NP0. With such a capacitor, the maximum deviation of the ratio (4), from the 25 ˚C value, is 2.09 %, whereas with the N805 capacitor, such deviation would be reduced to 1.33 %. However, note that the improvement is expected to be inferior if the whole range of temperature, until 90˚C, is taken into account. Given the non-linearity of the capacitance, another option is to use a non-linear dependent capacitor, for instance, a Z5U capacitor, whose temperature dependency is similar to the XLPE curve. This capacitor type has the disadvantage of a fast change in its nominal capacitance value with ageing. This would imply that the ratio of capacitances of (4) would be changing with time. This drawback discourages its use for compensating purposes.

B. Conclusions

The compensation method aims to determine off-line and experimentally the thermal drift of the cable capacitance and find the capacitor C_2 with the most suitable temperature coefficient so that the rate of capacitances remains as constant as possible regardless of the temperature. From the noise measurements, the temperature coefficient is -805 *ppm*. The

This article has been accepted for publication in a future issue of this journal, but has not been fully edited. Content may change prior to final publication. Citation information: DOI 10.1109/TPWRD.2015.2392386, IEEE Transactions on Power Delivery

model described in section III outputs the capacitance and temperature estimates plotted in Fig. 12.

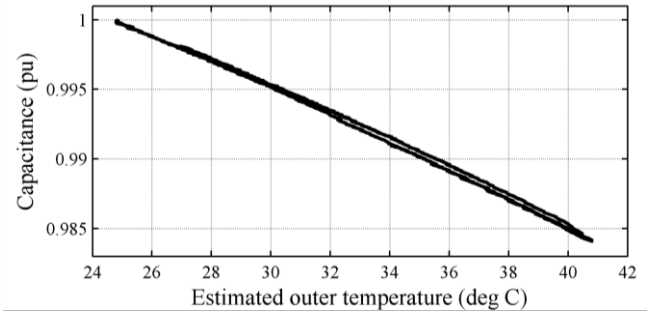

Fig. 12. Capacitance estimate vs outer temperature estimate.

The model outputs estimates which follow the same trend as the measurements. Both the estimated temperature and capacitance are similar. The TCC calculated from the model is -1008 *ppm*, leading to a difference of 20.1%. This significant difference is likely to be caused by several factors. One important factor is the measurement equipment that output important fluctuations in the measured capacitance lead to several outliers. Another important factor is the value of the physical *constants* of the materials in the embodiment. It is found that the linear thermal expansion coefficient of the XLPE material has great influence.

A big drawback for this method is the non-sensitivity of the method to difference cable conditions, i.e. the method is unable to distinguish between the scenario of high-current and low environment temperature and the scenario of low-current and high environment temperature, as far as the outer XLPE temperature is the same. These two scenarios would be compensated by C_2 in the same way. However, the XLPE relative permittivity is different in both scenarios. The compensation method 1 is unable to cope with such difference.

VI. Compensation Method 2

The second compensation method requires to measure the XLPE outer temperature, the electrical current and to use a zero temperature coefficient and stable capacitor C_2, for instance, a NP0 type. The objective is to build the complete thermal model above-mentioned in the digital signal processor and estimate the inner XLPE temperature. By doing this, the problem of the temperature difference can be overcome. For this reason, it is convenient to make use of a thermal-electric circuit analogy.

A. Thermal-Electric Analogy

An analogy between the thermal and the electrical magnitudes can be made in order to estimate the temperatures at different places in the sensor assembly. The thermal resistances are represented as electrical resistances, *R*, whereas the heat storage is represented by the corresponding capacitances, *C*. Moreover, it allows to include the heat sinks, by means of current sources. This analogy will be made to study the dynamics of the sensor system. Such an electrical circuit is shown in Fig. 13.

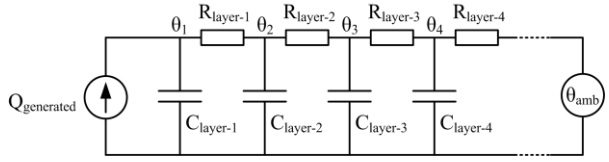

Fig. 13. Generic RC thermal circuit

The RC circuit of Fig. 13 has been modified, since the ambient temperature is not measured. Instead, the XLPE outer temperature is measured. Moreover, only 3 layers are considered: the aluminum central conductor, the inner semi-conductive layer and the XLPE insulation layer. The resistances, capacitances and heat sources have been detailed in the previous sections. The differential equations that govern such a linear RC-system are written in the form:

$$\dot{x} = M \cdot x + N \cdot u \tag{20}$$

Where x is the vector comprising the estimated temperatures of the outer aluminum and outer semi-conductive temperatures, $\dot{x}$ represents the vector with the corresponding time-derivatives *dx/dt*, u is the vector comprising the known or estimated terms: the generated heat (estimated from (9)) and the measured outer XLPE temperature, and *M* and *N* are the matrices that represent the circuit from Fig. 13:

$$M = \begin{bmatrix} \dfrac{-1}{R_{SC} \cdot C_{SC}} & \dfrac{1}{R_{SC} \cdot C_{SC}} \\ \dfrac{1}{R_{SC} \cdot C_{XL}} & \dfrac{-1}{C_{XL} \cdot (R_{SC} + R_{XL})} \end{bmatrix} \tag{21}$$

$$N = \begin{bmatrix} \dfrac{1}{C_{SC}} & 0 \\ 0 & \dfrac{1}{C_{XL} \cdot R_{XL}} \end{bmatrix} \tag{22}$$

Where the sub-index *SC* and *XL* next to the thermal resistances and capacitances stand for ”semi-conductive” and ”XLPE”. Such system can be solved with the Forward-Euler method, which needs the input of the initial conditions and can be easily solved in the digital processor.

$$x_{k+1} = x_k + \Delta t \cdot M \cdot x_k + \Delta t \cdot N \cdot u_k \tag{23}$$

Given the initial conditions, the geometry of the system can be initialized, the aluminum electrical resistance can be updated for the calculation of the generated heat, but also the thermal capacitances and resistances of the materials, since they also depend on the geometry. Given that the Forward-Euler method can be unstable, for stability and convergence of the results, the time step of 15 seconds used in the test has been reduced to 1.5 seconds by interpolation of the results.

B. Results

The Forward-Euler method has been applied to the very same scenario tested in the lab, with the same RMS current profile. Both the inner temperature of the XLPE layer, as well as the capacitive coupling, have been estimated in Fig. 14, according to the concepts and equations presented in the previous sections.

This article has been accepted for publication in a future issue of this journal, but has not been fully edited. Content may change prior to final publication. Citation information: DOI 10.1109/TPWRD.2015.2392386, IEEE Transactions on Power Delivery

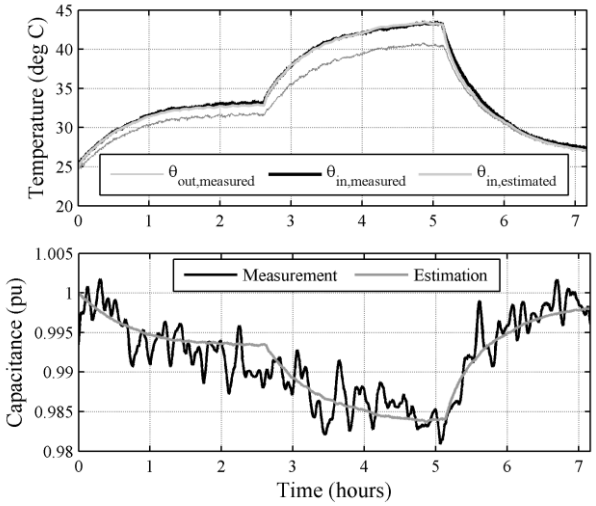

Fig. 14. Up: temperature estimation and measurement. Down: capacitance estimation and measurement

In general terms, the temperature approximation based on tabulated properties provides an accurate temperature estimation, which differs from the measurements by less than 1 ˚C. With such estimation, the average relative permittivity can be accurately estimated, considering the temperature difference between XLPE sides. Regarding the capacitive coupling, the estimation follows the same trend as the filtered measurements. Towards the actual implementation, in the analog part, the compensating capacitor C_2 would be of zero temperature coefficient, NP0 type. The method then uses a correction factor that takes into account the capacitance estimation, instead of considering a fixed value of the capacitances ratio in (4). This equation is now updated with the estimated values

$$\underline{V}_{out} \approx \frac{C_{1,estimated}}{C_{1,estimated}+C_2}\cdot\underline{V}_{in} = r_{estimated}\cdot\underline{V}_{in} \qquad (24)$$

The input voltage will be estimated by rearranging (24). The accuracy and performance of the method are evaluated by comparing the estimated ratio of capacitances ($r_{estimated}$) over the real ratio, obtained from the capacitance measurements $r_{real}=C_{1,real}/(C_{1,real}+C_2)$.

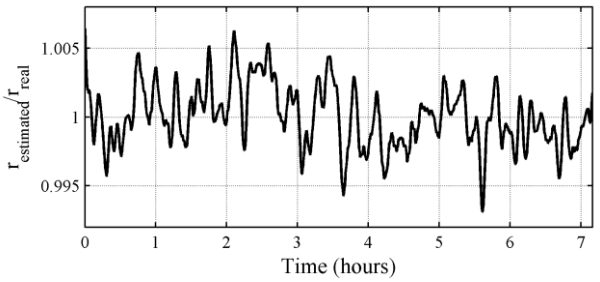

Fig. 15. Error in the ratio estimation with the obtained measurements

In Fig. 15, it can be seen that the estimated ratio of capacitances is kept between a range of 1.37 % with respect to the real ratio. This technique represents an improvement respect the case of no compensation at all. Much of the error is due to the uncertainty (noise) of the reference capacitance measurement from the LRC meter.

C. Conclusions

The second compensation method was designed to overcome the limitations of the first method, by measuring the electrode temperature and the conductor current and applying a corrected rate of capacitances. The results are improved with this method, obtaining a flatter rate of capacitances, which reduces the dependency of the sensor on the thermal drift. The application of the model outputs a capacitance estimate that follows the trend of the measurements and allows a deviation of about 1.37 %.

The application of the forward-Euler method requires some aspects to be considered: (i) the use of an appropriate time step to avoid instability, (ii) the initial conditions of temperature have to be input and (iii) an accurate characterization of the physical parameters.

Some limitations of the method are that (i) it requires an accurate definition both of the cable geometry and physical parameters; (ii) it may require some computational power to run the multi-physics estimation. However, as an advantage, this method can be applied along the whole range of temperatures, till 90 ˚C and takes into account the heat generation thermal distribution, which was lacking in the compensation method 1. An accurate mapping of the physical properties of the cable materials allows to develop a specific temperature-current model that keeps track on the cable geometry, the XLPE relative permittivity and the inner temperatures. Measuring the temperature at the outer XLPE layer allows one to omit the convection and radiation heat transfer mechanisms present on the cable outer surface layer.

VII. Discussion

A. Comparison of methods

The comparison between both methods, based on the range, does not show significant improvement from method 1 to method 2, actually the opposite. The range in method 1 is 1.33 %, whereas the range in method 2 is 1.37 %. However, the calculation of the range can be done exclusively by taking the spikes, which are dependent on the measurement equipment and its inaccuracy. The analysis of the variance of the rate can show how the rate remains steady along the test. Both the range and the variance of both methods are summarized in Table II, to be compared with the scenario of no compensation with a flat capacitor..

TABLE II
Comparison of methods

Compensation	Range (%)	Std deviation (%)
No: C_2 (NP0)	2.09	0.52
Method 1: C_2 (N805)	1.33	0.24
Method 2	1.37	0.22

The deviation of the results is inferior in the second method than the first one. This effect should be even more noticeable at higher temperatures, when the XLPE relative permittivity becomes less linear, with steeper falling slope.

This article has been accepted for publication in a future issue of this journal, but has not been fully edited. Content may change prior to final publication. Citation information: DOI 10.1109/TPWRD.2015.2392386, IEEE Transactions on Power Delivery

B. Eccentricity

Small variations in the geometry, together with thermal effects, can lead to significant changes in the thermal behavior. The eccentricity, according to Belgian standard HD 620 [22], is calculated as

$$Eccentricity = \frac{ti_{\min}}{ti_{\max}} \tag{25}$$

Where ti_{min} and ti_{max} are the minimum and maximum thickness. The standard defines two requirements for the eccentricity values, however, the one that applies for this case is an eccentricity inferior or equal to 0.85. Recall that the capacitance of a cable with eccentric geometry is given by [23]

$$C_{eccentric} = \frac{2\pi\varepsilon_0\varepsilon_r}{\ln\left(\frac{B^2 - d^2}{AB}\right)} \tag{26}$$

Where d is the distance between the insulation and the central conductor centers. The effect of the eccentricity produces an increase of the coupling capacity. Given that the cold shrink squeezes the cable cylindrical geometry, an asymmetrical distribution of the mechanical stresses can lead to an eccentricity between the central conductor and the semi-conductive and the XLPE layers. If the eccentricity stays constant during the temperature excursion, the effect can still be corrected with both methods. However, at higher temperatures, the XLPE layer becomes more viscous and, therefore, the geometry may be prone to small mis-alignments under mechanical stresses.

C. Phase error

A voltage sensor based on this capacitive coupling requires an electronic circuit to amplify and condition the tiny signal from the coupling. The electronic circuit may imply a high impedance load (R_{load}), in parallel with C_2. The capacitive coupling with the load becomes the circuit in Fig. 16.

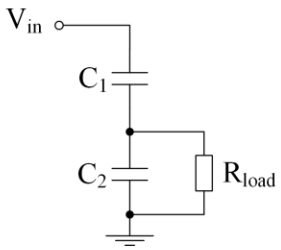

Fig. 16. Capacitive coupling with load resistance.

The connection of the load in parallel with C_2 leads to a phase error. The phase error is not negligible towards the fulfillment of the requirements of the standard IEC-60044-8 "*Instrument transformers - Electronic Current Transformers*", Annex D "*Frequency response and accuracy requirements on harmonics for electronic current and voltage transformer*" [24], that establishes the maximum phase error for power quality measurements, and for the different harmonics. The phase error is calculated as the angle of the ratio between impedances, according to (1). In this case, $\underline{Z}_2$ needs to be updated with the equivalent impedance $\underline{Z}_{eq}$, the parallel impedance of C_2 and R_{load}, as in

$$\text{phase error} = angle\left(\frac{\underline{Z}_{eq}}{\underline{Z}_1 + \underline{Z}_{eq}}\right) \tag{27}$$

The model introduced in this paper is applicable at the grid frequency. For this frequency, the standard defines a maximum phase error of ±18 mrad. Assuming C_1 equal to 17 pF and C_2 equal to 150 nF, the phase error at the grid frequency of 50 Hz is 21,2 mrad, beyond the limits. On the one hand, the compliance with the aforementioned standard can be used for sizing purposes. For instance, by increasing the value of C_2 from 150 nF up to the next standard value of 180 nF, the phase error becomes 17,7 mrad, now within limits. On the other hand, the thermal variations of C_1 do not affect significantly the phase error. Therefore, if the phase error is compensated, either with an appropriate C_2 or with a suitable electronic circuit, the thermal drift does not yield to a higher phase error.

D. Humidity

In [25], it has been described how humidity, in combination with other factors, such as high temperature or high frequency voltage, creates a harsh environment for the cable that contributes to the aging of the insulation. The experiments dealing with the XLPE degradation reproduce and sustain such harsh conditions to provoke the fast aging of the samples in a much shorter time. This degradation alters many properties of the XLPE material. The fast aging tests performed in [26], at 100 % relative humidity, 90 °C and 2 kV applied at the frequency of 50 Hz, reveal that the relative permittivity remained approximately constant during the first 500 hours. After 1000 hours, the values of relative permittivity started to fluctuate significantly, reaching the maximum variation around 3000 hours, and a relative permittivity 15 % inferior than the initial value. The thermal compensation methods presented in this paper would be unable to cope with the change of the permittivity under degradation. This limitation could be overcome with the monitoring the cable and updating of the properties.

VIII. Conclusions

In recent years, there has been an increased interest of DNOs in monitoring, not only the HV grid, but also some parts of the large MV distribution network. This requires the development of accurate, cheap and scalable sensors to be installed in an existing infrastructure. The voltage sensor studied in this paper was presented in the patents [1] and [2] and is to be installed in the terminations of XLPE underground cables, on top of the existing outer semiconducting layer, becoming a capacitive voltage divider. The accuracy of this sensor is compromised at high temperatures because of diverse multi-physics phenomena that take place while the cable is heated up.

This paper describes the geometry of the sensor assembly, the different phenomena that take place, and the manner the capacitive coupling varies with temperature: the change of resistivity in the Aluminum central conductor, the heat generation due to the current, the heat conduction through the

This article has been accepted for publication in a future issue of this journal, but has not been fully edited. Content may change prior to final publication. Citation information: DOI 10.1109/TPWRD.2015.2392386, IEEE Transactions on Power Delivery

different cable layers, the heat capacity of the material, the linear thermal expansion and the non-linear change of dielectric permittivity. This last phenomenon has been identified as of major importance to explain the cable capacitance change. This change of capacitance is to be compensated in order to increase the accuracy of the sensor, and, therefore, two methods have been investigated. Both methods require the knowledge of the temperature at the outer surface of the XLPE layer. The capacitance and the inner and outer temperatures of the XLPE have been measured in an experimental test, where the temperatures are brought up to the steady-state when a 300 A current flows.

The first method consists of characterizing the change of cable capacitance as function of the outer XLPE temperature. This behavior has been linearly approximated, determining the temperature coefficient of an external capacitor that will passively compensate the thermal drift. This characterization has been done in the range between 24 to 41 ˚C and the method shows an improvement with respect to the case of no compensation. However, because of the non-linear behavior of the XLPE relative permittivity, this method may show limited improvement if the whole temperature range (till 90 °C) is used for characterization. The method is insensitive to the heat transfer direction, but also to the important difference of temperature between the inner and the outer side of the XLPE layer.

Given the sharp change of the XLPE relative permittivity with temperature, a big difference of temperatures between both sides of the layer can lead to significant deviations in the over-all permittivity value. The second method attempts to resolve this aspect by estimating the inner temperature of the XLPE. This requires to measure the outer XLPE temperature, as well as the electrical current through the conductor. The capacitive coupling model, described by its multi-physics equations, is to be implemented digitally. The thermal-electrical RC equivalent circuit is used to study the transient thermal behavior of the temperatures, while the forward- Euler method allows one to solve the linear circuit and to obtain a temperature approximation. Based upon the temperature estimation, the XLPE relative permittivity, the capacitive coupling, the rest of variables are estimated. Within the tested range of temperatures, both methods show a similar improvement. In both cases, the improvement is masked by the noise in the capacitance measurements. In spite, the second method is designed to provide better performance than the first one. It also requires a precise knowledge about the material properties and geometry, but it is able to compensate the deviations of the capacitive coupling over a wider range of temperatures and current flow.

It is also shown that a load connected to the capacitive coupling leads to a phase error. However, the model predicts that the thermal drift of the cable does not change significantly the phase error. Moreover, the phase error can be reduced by sizing appropriately C_2, therefore, the compliance with the standard [24] can be used as an optimization criterion.

IX. Acknowledgment

The authors want to express their gratitude to Ruben Gielen, Jonathan Crabbé and Jeroen Tant. Sam Weckx has a PhD fellowship of the Research Foundation - Flanders – VITO (FWO-VITO).

X. References

[1] T. De Rybel and E. Vandewinckel, ”Guarding methods for high voltage measurements,” European Patent 2 508 898, 2012.

[2] T. De Rybel and E. Vandewinckel, ”High voltage measurement systems,” European Patent 2 689 256, 2014.

[3] J. Trott, ”Capacitive voltage divider for high-voltage cables,” German Patent 3 702 735, 1988.

[4] C. Weinmann, H. Kurzhals, M. Stalder, S. Eggert and J. Weichold, ”Sensored cable for a Power Network,” WO 096 424, 2013.

[5] G. Bolcato, J. Weichold, P. Zanoli, M. Gravermann, M. Stalder, H. Kurzhals, S. Eggert and C. Weinmann, ”Terminal Connection Device for a Power Cable,” WO 096 354, 2013.

[6] T.J.D. Heyer, R.A. Wandmacher and L. C. Chor and J.T. Larson, ”Stress control for termination of a high voltage cable,” U.S. Patent 6 015 629, 2000.

[7] T. Hobejogi and J. Biela, ”Coaxial capacitive voltage divider with high division ratio for high voltage pulses with very fast rise times,” in *2011 Pulsed Power Conference (PPC)*.

[8] P. Johansen, ”Substation Automation,” 2008 *CIRED* Seminar: Smart Grids for Distribution.

[9] Jin-Liang Liu, Ye Bing, Zhan Tian-Wen, Feng Jia-huai, Zhang Jian-De, Wang Xin-Xin, ”Coaxial Capacitive Dividers for High-Voltage Pulse Measurements in Intense Electron Beam Accelerator With Water Pulse-Forming Line,” *IEEE Trans. Instrumentation and Measurement*, vol.58, no.1, pp.161,166, Jan. 2009.

[10] D. A. Tziouvaras, P. McLaren, G. Alexander, D. Dawson, J. Esztergalyos, C. Fromen, M. Glinkowski, I. Hasenwinkle, M. Kezunovic, L. Kojovic, B. Kotheimer, R. Kuffel, J. Nordstrom and S. Zocholl, ”Mathematical models for current, voltage, and coupling capacitor voltage transformers,” *IEEE Trans. Power Delivery*, vol.15, no.1, pp.62,72, Jan 2000.

[11] J. Izykowski, B. Kasztenny, E. Rosolowski, M.M. Saha, B. Hillstrom, ”Dynamic compensation of capacitive voltage transformers,” *IEEE Trans. on Power Delivery*, vol.13, no.1, pp.116,122, Jan 1998.

[12] R.M. Eichhorn, ”A Critical Comparison of XLPE-and EPR for Use as Electrical Insulation on Underground Power Cables,” *IEEE Trans. Electrical Insulation*, vol.EI-16, no.6, pp.469,482, Dec. 1981.

[13] *Electrical Power Cable Engineering*, W.A. Thue, Ed. Marcel Dekker, Inc. Washington, D.C., 1999.

[14] C. Garrido, A.F. Otero and J. Cidras, ”Theoretical model to calculate steady-state and transient ampacity and temperature in buried cables,” *IEEE Trans. Power Delivery*, vol.18, no.3, pp.667,678, July 2003.

[15] Yanmu Li, Yongchun Liang, Yanming Li, Wenrong Si, Peng Yuan and Junhao Li, ”Coupled Electromagnetic-Thermal Modeling the Temperature Distribution of XLPE Cable,” in *Proc. 2009 Power and Energy Engineering Conf. Asia-Pacific* , pp.1,4, 27-31.

[16] M.S. Al-Saud, M.A. El-Kady and R.D. Findlay, ”Combined simulation experimental approach to power cable thermal loading assessment,” *IET Generation, Transmission & Distribution*, vol.2, no.1, pp.13,21, Jan. 2008.

[17] Mazzanti, G., ”Analysis of the Combined Effects of Load Cycling, Thermal Transients, and Electrothermal Stress on Life Expectancy of High-Voltage AC Cables,” *IEEE Trans. Power Delivery*, vol.22, no.4, pp.2000,2009, Oct. 2007.

[18] D. Carstea and I. Carstea, ”Simulation of coupled electric and thermal fields in coaxial cables,” in *Proc. 2003 Telecommunications in Modern Satellite, Cable and Broadcasting Service International Conf.*, pp.697,700.

[19] R. Strobl, W. Haverkamp, G. Malin and F. Fitzgerald, ”Medium voltage terminations using an advanced stress control technology,” in *Proc. 2001 IEEE/PES Transmission and Distribution Conf. and Exposition*, pp.771,775.

[20] K. Väkeväinen, "The effect of material properties to electric field distribution in medium voltage underground cable accessories," MSc dissertation, 2010.
[21] J. H. Lienhard IV, J. H. Lienhard V, *A heat transfer textbook*, Phlogiston Press, Cambridge, Massachusetts, 3rd edn, 2008.
[22] HD 620, "Distribution cables with extruded insulation for rated voltages from 3.6/6(7.2)kV to 20.8/36(42)kV," 3rd edition, 2007.
[23] *Power Cables and their Application, part 1*, Edited by Lothar Heinhold, Siemens Aktiengesellschaft, Berlin and Munich, Germany, 3rd revised edition, 1990.
[24] Std IEC-60044-8, "Instrument transformers – Electronic Current Transformers", Annex D, "", 2002-07.
[25] S.V.Nikolajevic, "Investigation of water effects on degradation of Crosslinked polyethylene (XLPE) insulation" *IEEE Trans. Power Delivery*, vol. 8, no.4, pp. 1683-1688, Oct. 1993.
[26] Y. Mecheri, M. Nedjar, A. Lamure, M. Aufray, C. Drouet, "Influence of Moisture on the Electrical Properties of XLPE Insulation," *Annual Report Conference on Electrical Insulation and Dielectric Phenomena*, 2010.

XI. BIOGRAPHIES

Carlos Gonzalez (S'10) received his M. Sc in Electrotechnics at the Polytechnic University of Catalonia (UPC, Barcelona Tech) in 2009. From 2006 till 2010, he was a researcher at CITCEA - UPC and IREC, Barcelona. Since 2010, he is a Ph.D. student and research assistant at ESAT-ELECTA in the Katholieke Universiteit Leuven (KULeuven), Belgium. His research interests include power quality in smart grids and fault detection.

Sam Weckx (S'11) received the M.Sc. degree in Electrical Engineering in 2009 and Mechanical Engineering in 2010 from the Katholieke Universiteit Leuven (KU Leuven), Belgium, where he is currently working towards the Ph.D. degree as a research assistant with the division ESAT-ELECTA. His research interests include the application of distributed optimization in smart grids and voltage control in distribution networks.

Tom De Rybel received the Industral Engineer degree in electronics design from Hogeschool Gent, Belgium, in 2002 and the M.A.Sc and PhD degrees in power systems from the University of British Columbia, Vancouver, Canada, in 2005 and 2010, respectively. His research interests, as a post-doctoral fellow at KU Leuven, Belgium, include smart-grid component design, high-voltage instrumentation, asset condition monitoring, power electronics, numerical acoustics, and hardware-in-the-loop simulation.

Johan Driesen (S93 - M97 SM12) received the M.Sc. and Ph.D. degrees in Electrical Engineering from the Katholieke Universiteit Leuven (KU Leuven), Leuven, Belgium, in 1996 and 2000, respectively. Currently, he is a Professor with the KU Leuven and teaches power electronics and electric drives. In 2000, he was with the Imperial College of Science, Technology and Medicine, London, U.K. In 2002, he was with the University of California, Berkeley. Currently, he conducts research on distributed generation, power electronics, and its applications.